JOURNAL OF Materials CHEMISTRY

Fluorescence enhancement and structural development of sol–gel derived Er^{3+}-doped SiO_2 by yttrium codoping

San-Yuan Chen,* Chu-Chi Ting and Chia-Hou Li

Department of Materials Science and Engineering National Chiao-Tung University, 1001 Ta-hsueh Road, Hsinchu 300 Taiwan, Republic of China. E-mail: sychen@cc.nctu.edu.tw; Fax: 886-3-5725490; Tel: 886-3-5731818

Received 13th August 2001, Accepted 22nd January 2002
First published as an Advance Article on the web 4th March 2002

Er^{3+}–Y^{3+} codoped SiO_2 powdered bulks were prepared by a sol–gel process. The effect of Y^{3+} codoping on the fluorescence properties and structural development of Er^{3+}-doped SiO_2 is investigated. The maximum ~1.54 μm photoluminescence (PL) intensity occurs in the sample with Er^{3+} (10 mol%)–Y^{3+} (50 mol%) codoped and annealed at 985 °C. This can be attributed to the competition between the content of hydroxy groups and Er site symmetry. Improvement of optimum PL properties due to Y^{3+} codoping by a factor of ~20 for intensity and 1.8 for the full width at half maximum (57 nm) was obtained in comparison with the Er^{3+}-doped SiO_2 system. Extended X-ray absorption fine structure analysis shows that the local chemical environment of Er^{3+} ions in the Er^{3+}–Y^{3+} codoped SiO_2 is similar to that in Er_2O_3. The average spatial distance between Er^{3+} ions is enlarged due to a partial substitution of Y^{3+} for Er^{3+} ions in the Er_2O_3-like local structure, which results in a reduction of the concentration quenching effect.

1. Introduction

Rare-earth doped materials play very important roles in optoelectronics technology because they have good performance in the application of lasers and optical amplifiers.[1–3] Among these rare-earth elements, the ~1.54 μm photoluminescence (PL) properties of Er^{3+} ions are of particular interest in fiber optical communication systems because it matches the lowest signal attenuation in silica-based optical fibers.[4,5]

The ~1.54 μm PL efficiency was strongly influenced by some factors such as the local symmetry of Er^{3+} sites in the host matrix, the concentration quenching effect, and the content of hydroxy impurities (OH^-) in the sol–gel derived materials.[6,7] In the case of free Er^{3+} ions, the ~1.54 μm optical emission of internal 4*f*–4*f* transitions (between the $^4I_{13/2}$ first excited and the $^4I_{15/2}$ ground state) is electric dipole forbidden. If the symmetry of the local crystal field around the Er^{3+} lattice sites in the host matrix is distorted, the parity forbidden intra-4*f* transition will be allowed.[8,9] Additionally, for a high Er^{3+} doping, the Er^{3+} ions tend to form clusters and the mean interaction distance between Er^{3+} ions becomes small, which results in substantial losses of excitation energy through the ion–ion interaction mechanism (*e.g.*, co-operative up-conversion cross-relaxation and resonant energy migration) between the two nearby Er^{3+} ions. In other words, the chemical environment of Er^{3+} ions (*i.e.* the site symmetry and clustering of Er^{3+} ions) in the host matrix significantly affects the luminescence efficiency. Therefore, the addition of specific heteroatoms into the host matrix to reduce the site symmetry and clustering of Er^{3+} ions will be the most efficient method to promote the ~1.54 μm PL intensity. For instance, it is well known that the solubility of Er^{3+} ions in silicate hosts is very low. Many researchers have tried to codope Al^{3+} or P^{3+} ions with Er^{3+} ions into a silicate host in order to provide enough non-network oxygen species and hence decrease the concentration quenching effect.[10–13] The addition of co-dopants Al^{3+} or P^{3+} ions has focused on the modification of the host matrix to improve the Er solubility. However, the structural role of Er in the host matrix has been neglected.

Y^{3+}/Er^{3+} ions have similar ionic radii (Y^{3+} = 0.0892, and Er^{3+} = 0.0881 nm) and Y_2O_3/Er_2O_3 have nearly the same crystal structure and lattice constant. Therefore, we have tried to codope Y^{3+} ions into the Er^{3+}-doped SiO_2 network by the sol–gel method in the present work. The role of the Y^{3+} codopant in the phase development and PL properties of Er^{3+}-doped silica materials will be investigated. Additionally, the extended X-ray absorption fine structure (EXAFS) technique will be used to analyze the influence of Y^{3+} ions on the local chemical environment around the Er^{3+} ions in an Er^{3+}–Y^{3+} codoped SiO_2 system.

2. Experimental

2.1. Sample preparation

TEOS [tetraethoxysilane, $Si(OC_2H_5)_4$, Merck, 99.5%] was used as the silicon alkoxide precursor for all of the Er^{3+}-doped samples. Erbium nitrate pentahydrate [$Er(NO_3)_3{\cdot}5H_2O$, Alfa, 99%], and yttrium nitrate pentahydrate [$Y(NO_3)_3{\cdot}5H_2O$, Alfa, 99%] were used as the sources of Er^{3+} and Y^{3+} ions, respectively. TEOS was first added to the mixture solution of deionized water and ethanol (Merck, 99.9%) (the molar ratio of $TEOS : H_2O : C_2H_5OH = 1 : 5 : 10$), followed by stirring for 30 min. Then the erbium solution (erbium nitrate : H_2O = 1 : 10) and yttrium solution (yttrium nitrate : H_2O = 1 : 10) were spontaneously dropped into the initial TEOS solution. This sol solution was vigorously stirred at room temperature for 10 h in order to ensure a sufficient degree of hydrolysis and polycondensation. Molar ratios of Er^{3+} and Y^{3+} (relative to Si^{4+}) ranging from 0.5 to 10% and 10 to 50% were used, respectively.

The final sol solutions were aged at room temperature for 6 days and gelled at 50 °C in about 2 weeks. Gels were heat-treated at 100 °C in air for 6 days and were then pyrolyzed at 700 °C for 1 h in a dry oxygen atmosphere at a heating rate of 2 °C h^{-1} to remove organic species. Pyrolyzed gel powder was die-pressed to be a 1 cm-diameter pellet and then annealed at 800–1400 °C for 1 h in a dry oxygen atmosphere at a heating rate of 10 °C min^{-1}.

 DOI: 10.1039/b107380j

2.2. Characterization measurements

The phase structure of the samples was determined by an X-ray diffractometer (MAC Science, M18X) using Cu-Kα radiation. Fourier transform infrared (FTIR) spectra were recorded on a Perkin–Elmer 580 spectrometer. A transmission electron microscope (TEM, JEOL-2000FX) equipped with EDX was used to observe and analyze the microstructure. The fluorescence spectra were excited by a 980 nm laser diode with a power of 50 mW inclined 45° to irradiate the samples and recorded normally from the samples using a spectrophotometer equipped with a liquid N_2-cooled Ge detector (NCSC).

Erbium L_{III}-edge X-ray absorption spectra were recorded on Wiggler beamline S-05B at the Synchrotron Radiation Research Center (SRRC), Hsinchu, Taiwan. The electron storage ring was operated at an energy of 1.3 GeV and a current of 80–200 mA. A Si (111) double-crystal monochromator with a 0.5 mm entrance slit was used for energy scanning. The energy resolution, $\Delta E/E$, was about 1.9×10^{-4}. Measurements were performed at room temperature in fluorescence mode and the sample was positioned at 45° to the incident X-ray beam. A polycrystalline Er_2O_3 powder (Cerac, 99.9%) was used as a reference standard.

3. Results

The X-ray diffraction (XRD) patterns in Fig. 1 illustrate the effect of the annealing temperatures on the structural evolution of pure SiO_2, Er^{3+}-doped SiO_2 and Y^{3+}-doped SiO_2, where the silicate host codoped with Er^{3+} (20 mol%)–Y^{3+} (0 mol%) and annealed at 1100 °C is denoted as "Er20 Y0 1200 °C". For annealing temperatures below 1300 °C, the pure SiO_2 host exhibits an amorphous structure. The polymorphic SiO_2 is detectable when the annealing temperature exceeds 1400 °C. When 10 mol% Er^{3+} ions were added into the SiO_2 matrix, it was found that phase crystallization occurs at 1100 °C. With increasing Er^{3+} concentration up to 20 mol%, the well-defined crystalline phase can be clearly identified as the Er-pyrosilicate phase ($Er_2Si_2O_7$).[14] On the other hand, Y^{3+}-doped SiO_2 exhibits similar crystallization behavior to Er^{3+}-doped SiO_2 and also forms the polymorphic Y-pyrosilicate phase ($Y_2Si_2O_7$) at 1100 °C.[15] Notedly, both $Er_2Si_2O_7$ and $Y_2Si_2O_7$ phases have almost the same XRD patterns, which means that both Er- and Y-pyrosilicates have the same crystal structure and nearly the same lattice constant.

The effect of yttrium concentration on the phase evolution of the Er^{3+} (5 mol%)-doped SiO_2 at different annealing temperatures is shown in Fig. 2. When annealed at 985 °C/1 h, even though as high as 50 mol% Y^{3+} was added into the Er^{3+}-doped SiO_2, the XRD pattern shows an amorphous

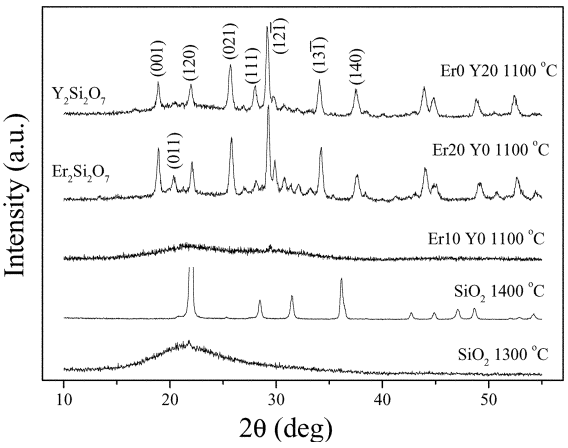

Fig. 1 X-Ray diffraction patterns of SiO_2 and Er^{3+} (or Y^{3+})-doped SiO_2 samples annealed at different temperatures for 1 h.

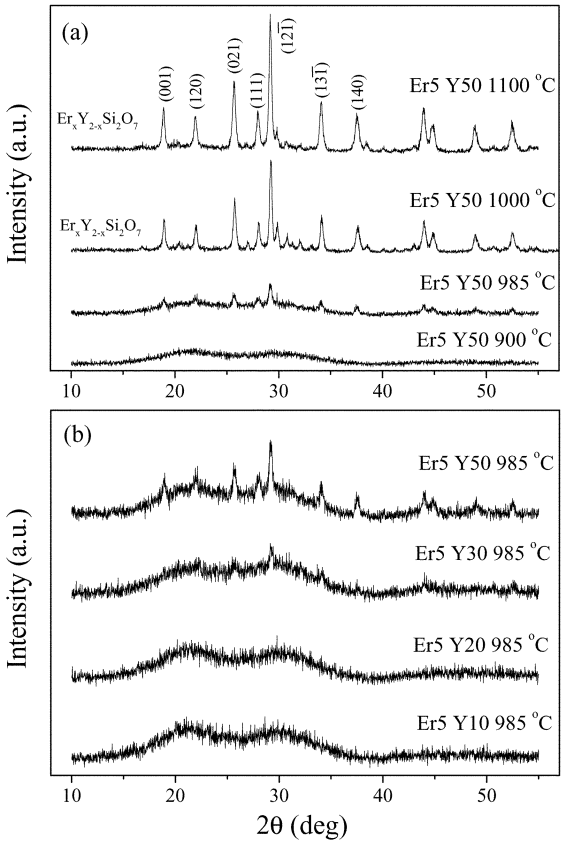

Fig. 2 X-Ray diffraction patterns of Er^{3+} (5 mol%)–Y^{3+} codoped SiO_2 samples (a) annealed at temperatures of 900–1000 °C/1 h, and (b) with different Y^{3+} concentration and annealed at 985 °C/1 h.

structure. The relationship between the total Er^{3+} + Y^{3+} codoping concentration and annealing temperatures for the crystallization behavior of Er^{3+}–Y^{3+} codoped SiO_2 samples is further summarized in Fig. 3. For example, when the total concentration of Er^{3+} and Y^{3+} ions is more than 30 mol%, the crystalline phase ($Er_xY_{2-x}Si_2O_7$) will be generated for all of the samples annealed at 985 °C.

Fig. 4 shows the FTIR spectra of the Er^{3+}–Y^{3+} codoped SiO_2 samples annealed at 800 and 1000 °C for 1 h. The FTIR spectrum of Er^{3+} (5 mol%)–Y^{3+} (10 mol%) codoped SiO_2 annealed at 800 °C is found to be similar to that of the pure silicate. The bands around 1079 cm^{-1} and 796 cm^{-1} correspond to the Si–O–Si antisymmetrical and symmetrical stretching vibrations, respectively.[16,17,18] The band around 455 cm^{-1} is due to the Si–O–Si and O–Si–O bending modes.[18–20] However, with increasing Y^{3+} concentration (from 30 to

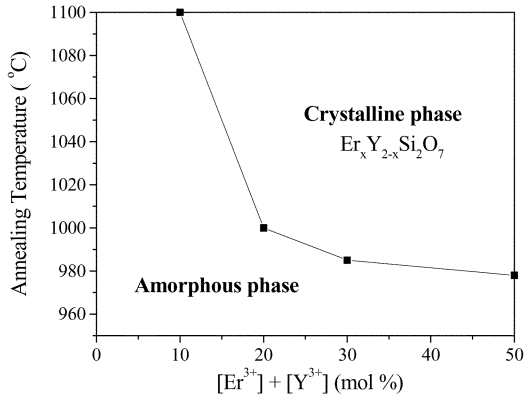

Fig. 3 Dependence of crystallization behavior of Er^{3+}–Y^{3+} codoped SiO_2 samples on total Er^{3+} + Y^{3+} codoping concentration and annealing temperatures.

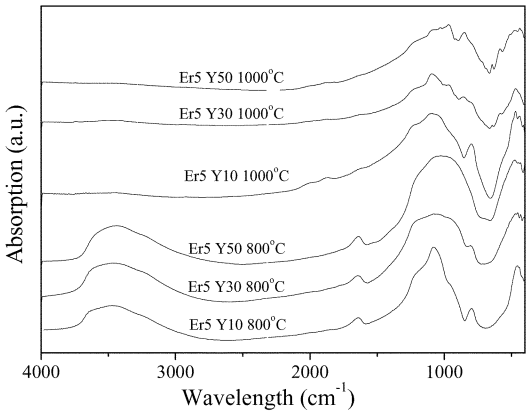

Fig. 4 FTIR absorption spectra of Er^{3+}–Y^{3+} codoped SiO_2 samples annealed at different temperatures for 1 h.

50 mol%), the band around 1079 cm^{-1} becomes broad and the band around 796 cm^{-1} gradually weakens and disappears. This reveals that the network structure of short-range order tetrahedral SiO_4 was destroyed and became more disordered. In addition, all of the samples exhibit a broad absorption in the 3000–3450 cm^{-1} region (the O–H stretching vibration) and a small band at $\sim$1620 cm^{-1} (the molecular H–O–H bending mode).[18,21,22] This indicates that there exists a variety of hydroxy groups such as isolated Si–OH groups, pairs of hydrogen bonded Si–OH and physically adsorbed water molecules in the silica matrix.[18,21,22]

As the sample was annealed at 1000 °C, some newly-formed peaks at 585, 851, 966 and 1084 cm^{-1} in the FTIR spectra were observed for the samples with a Y^{3+} concentration above 30 mol% that could be related to the formation of the crystalline pyrosilicate $Er_xY_{2-x}Si_2O_7$ phase. However, the assignment of these peaks is not the focus of this paper. Additionally, the absorption bands around 3000–3450 and 1620 cm^{-1} have obviously disappeared. Since the content of hydroxy quenching centers is sensitive to the annealing temperature, the FTIR spectra in the range of 4000–3000 cm^{-1} (where the intensity of absorption bands represents the content of hydroxy groups) were performed for the Er^{3+} (5 mol%)–Y^{3+} (50 mol%) codoped SiO_2 samples annealed at 800–1000 °C. Fig. 5 illustrates that the content of hydroxy groups is rapidly reduced with an increase of annealing temperature from 970 to 1000 °C.

Fig. 6 illustrates the $\sim$1.54 μm PL spectra of the Er^{3+} (1 and 5 mol%)–Y^{3+} (0–50 mol%) codoped SiO_2 samples annealed at 985 °C for 1 h. These spectra exhibit a broad PL emission that consists of a $\sim$1.538 μm main peak and some broad shoulders. Moreover, the spectral bandwidths also become enlarged with

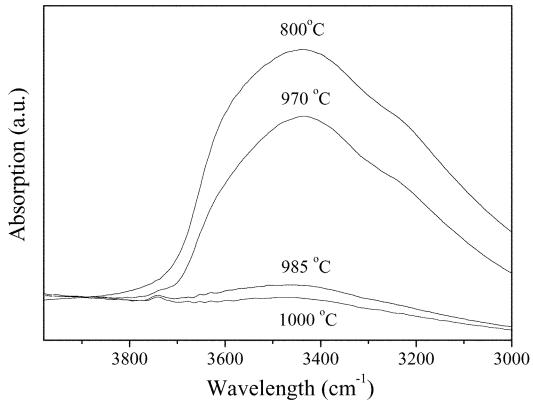

Fig. 5 FTIR absorption spectra between 4000 and 3000 cm^{-1} showing the effect of annealing temperature on the hydroxy content of Er^{3+} (5 mol%)–Y^{3+} (50 mol%) codoped SiO_2 samples.

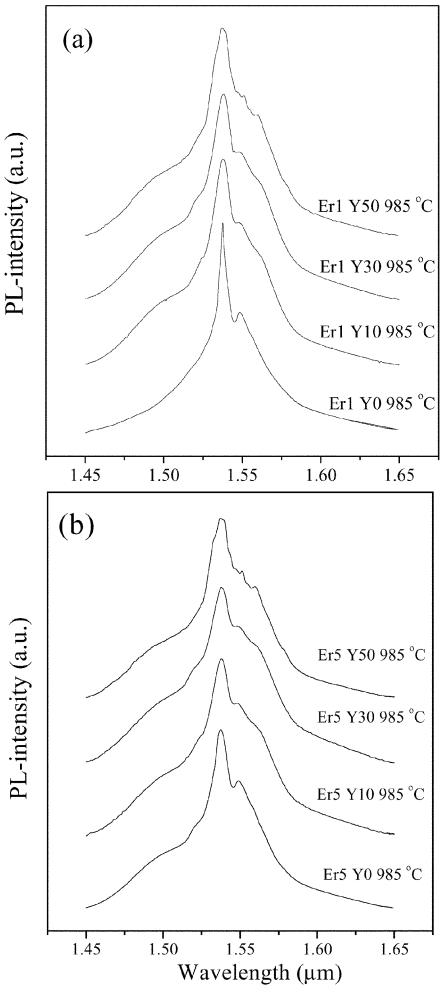

Fig. 6 $\sim$1.54 μm PL spectra of (a) Er^{3+} (1 mol%) and (b) Er^{3+} (5 mol%)–doped SiO_2 samples with different Y^{3+} concentration codoped and annealed at 950 °C for 1 h. All of the spectra are normalized on the same basis of intensity for comparison among spectral features.

more Y^{3+} codopant being added. Fig. 7 shows the annealing temperature dependence of the $\sim$1.54 μm PL spectra observed from the Er^{3+} (5 mol%)–Y^{3+} (50 mol%) codoped SiO_2 samples. The broad PL spectra will split into many sharp lines when the crystalline $Er_xY_{2-x}Si_2O_7$ phase is generated in the host matrix at 1000 °C.

The effect of annealing temperature on the PL intensity of the Er^{3+} (1–10 mol%)–Y^{3+} (50 mol%) codoped SiO_2 samples is further illustrated in Fig. 8. The results reveal that the PL intensities were enhanced with increasing annealing temperatures from 800 to 985 °C, while it decreased above 1000 °C. The dependence of Er^{3+} and Y^{3+} concentration on the PL intensity of Er^{3+}–Y^{3+} codoped SiO_2 samples annealed at 985 °C for 1 h is schematically summarized in Fig. 9. The PL intensity of the Er^{3+} (5 and 10 mol%)–Y^{3+} codoped SiO_2 samples increases remarkably with the increase of the Y^{3+} codoping level. However, for the Er^{3+} (1 mol%)–Y^{3+} codoped SiO_2 samples, the PL intensities are slightly reduced when the Y^{3+} codoping level exceeds 30 mol%. Notably, the PL intensity of the Er^{3+} (5 and 10 mol%)-doped SiO_2 sample can be increased by a factor of almost 20 in the presence of 50 mol% Y^{3+} codopant, demonstrating that Y^{3+} codoping is a very efficient method for enhancing the PL intensity in the Er^{3+}-doped SiO_2 system.

Fig. 10 shows the pseudo-radial distribution functions obtained from the k^3-weighted Fourier transforms of the Er^{3+}–Y^{3+} codoped SiO_2 samples annealed at 900–1000 °C for 1 h. Qualitative observation reveals that the first-neighbor

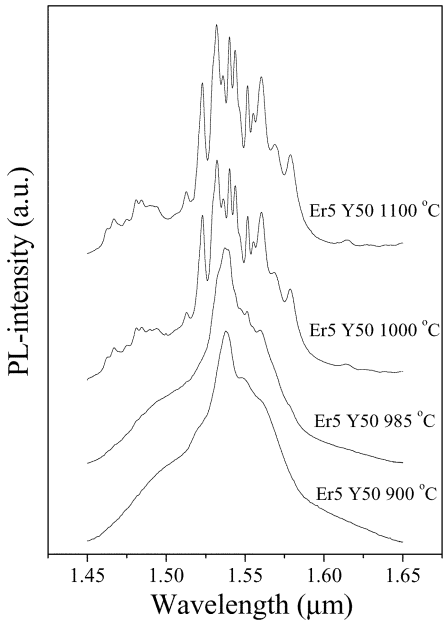

Fig. 7 ~1.54 μm PL spectra of Er^{3+} (5 mol%)–Y^{3+} (50 mol%) codoped SiO_2 samples annealed at 900–1100 °C for 1 h. All of the spectra are normalized on the same basis of intensity for comparison among spectral features.

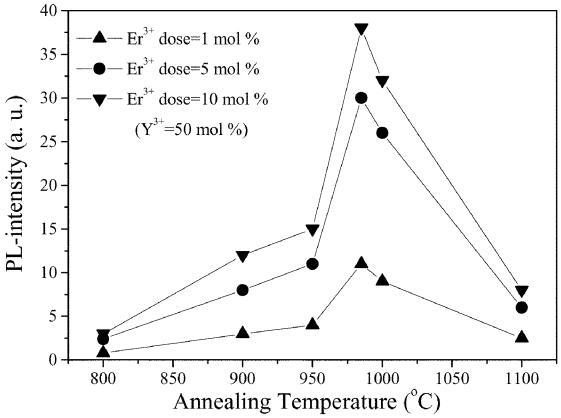

Fig. 8 PL intensity of Er^{3+}–Y^{3+} (50 mol%) codoped SiO_2 samples as functions of Er^{3+}content and annealing temperatures.

distance of Er^{3+} at 900 °C is similar to that of the crystalline Er_2O_3, indicating that the first neighbors of Er^{3+} ions are primarily composed of O atoms. The second nearest neighbor distance of Er^{3+} is close to the distance of the second nearest

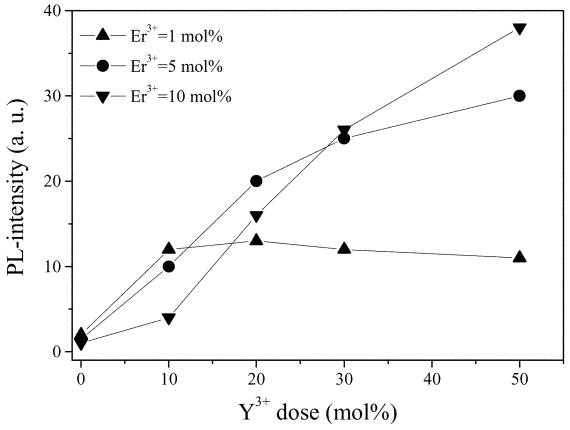

Fig. 9 Dependence of Er^{3+} and Y^{3+} concentration on the PL intensity of Er^{3+}–Y^{3+} codoped SiO_2 samples annealed at 985 °C for 1 h.

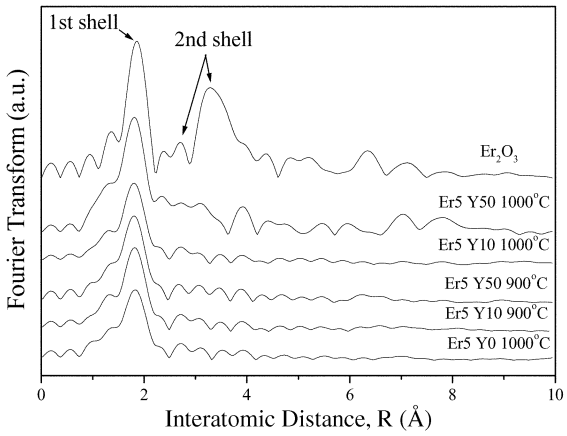

Fig. 10 Fourier transform partial radial distribution function for the Er^{3+}–Y^{3+} codoped SiO_2 samples annealed at 900–1100 °C for 1 h.

neighbor in Er_2O_3. Therefore, the local chemical environment of Er^{3+} ions in the amorphous Er^{3+}–Y^{3+} codoped SiO_2 samples is an Er_2O_3-like environment. At 1000 °C, the EXAFS curves of the Er^{3+} (5 mol%)–Y^{3+} (50 mol%) codoped SiO_2 samples illustrate that the first shell is like that of Er_2O_3 but its outer shells are obviously different from those of amorphous samples because the coordination number of the Er^{3+} ion in the well-crystalline $Er_xY_{2-x}Si_2O_7$ phase is still 6-fold.[23,24]

4. Discussion

4.1. Influence of Y^{3+} content and annealing temperature on the PL properties

When the Er^{3+} (1–10 mol%)–Y^{3+} (0–50 mol%) codoped SiO_2 samples were annealed at 950 °C, all of them have an amorphous structure and all exhibit similar broad PL spectra (see Fig. 6). However, there still existed an apparent difference in FWHM between these spectra. The FWHM is ~45 nm for the Er^{3+} (1 mol%)–Y^{3+} (10 mol%) codoped SiO_2, which is larger than that of the Er^{3+} (1 mol%)-doped SiO_2 without the Y^{3+} codopant (FWHM = ~31 nm). The broadening of the PL spectra indicates that the Y^{3+} codopant plays a modifier role in affecting the bonding environment of Er^{3+} ions that can lead to a wider diversity of Er^{3+} bonding sites. However, for Er^{3+} (1 mol%)–Y^{3+} codoped SiO_2 samples with a Y^{3+} concentration varying form 10 to 50 mol%, the spectral bandwidth does not show an apparent difference. This implies that 10 mol% Y^{3+} codoping is enough to modify the Er bonding environment and maximize the Er site diversity in the SiO_2 matrix. The above-mentioned phenomenon is also observed for the Er^{3+}–Y^{3+} codoped SiO_2 samples with a larger amount of Er^{3+} (5–10 mol%). The full width at half maximum (~57 nm) is also larger than that (~40 nm) of the Er^{3+} (5–10 mol%)-doped SiO_2 without Y^{3+} codoping.

The phase evolution of Er^{3+}–Y^{3+} codoped SiO_2 samples is strongly dependent on the Er^{3+} + Y^{3+} concentration and annealing temperature. As shown in Fig. 3, for the samples with an Er^{3+} + Y^{3+} concentration greater than 30 mol% and annealed above 985 °C, the highly crystalline $Er_xY_{2-x}Si_2O_7$ phase forms in the host matrix. The TEM micrograph of an Er^{3+} (5 mol%)–Y^{3+} (50 mol%) codoped SiO_2 sample annealed at 1000 °C shows that many dark small droplet precipitates were observed (Fig. 11).[25–27] The energy-dispersive X-ray (EDX) analysis reveals that these precipitates contain Er and Y elements. As compared with XRD patterns (Fig. 2(a)), these precipitates should be the $Er_xY_{2-x}Si_2O_7$ phase. This indicates that most of the Er^{3+} ions are located on the well-defined sites of the $Er_xY_{2-x}Si_2O_7$ phase. Therefore, a number of sharp PL lines were observed as shown in Fig. 7.

Since both the content of hydroxy groups (*i.e.*, quenching

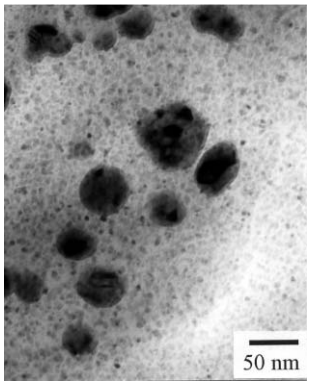

Fig. 11 TEM micrograph of Er^{3+} (5 mol%)–Y^{3+} (50 mol%) codoped SiO_2 annealed at 1000 °C for 1 h.

centers) and the symmetry of local structure around the Er^{3+} ions can affect the PL intensity, the final-revealed PL intensity results from the competition between these two factors. For the samples annealed at 970 °C (*i.e.*, no crystalline $Er_xY_{2-x}Si_2O_7$ phase existing in the host matrix), the varying PL intensity is primarily related to the amount of OH^- hydroxy impurities. Therefore, in the temperature range 800–970 °C, the PL enhancement with increasing annealing temperature is mostly attributed to the decrease of the hydroxy quantity.[28–31]

When the annealing temperature reached 985 °C, the poorly crystalline $Er_xY_{2-x}Si_2O_7$ phase had formed in the host matrix and resulted in the reduction of the probability of the $^4I_{13/2} \rightarrow {}^4I_{15/2}$ transitions. However, a maximum PL intensity was observed at this temperature (985 °C) that reveals that the greatly decreased content of hydroxy quenching centers (see Fig. 5) can still offset the influence of the higher local symmetry of the Er site. On the other hand, as the samples were annealed at higher temperatures above 1000 °C, the $Er_xY_{2-x}Si_2O_7$ phase has been highly crystallized and thus the local structure around the Er^{3+} ions becomes more symmetric. Therefore, an abrupt reduction of the PL intensity is observed.

4.2. Role of Y^{3+} codopant on the development of Er^{3+} local structure

EXAFS analysis in Fig. 10 shows that there is local Er_2O_3-like structure in the amorphous Er^{3+}–Y^{3+} codoped SiO_2 host matrix. These Er sites with Er_2O_3-like local symmetry are generally thought of as the active luminescent centers.[32–34] Because Er^{3+} and Y^{3+} have the same valence and similar ionic radii (0.0881 and 0.0892 nm, respectively), they could be replaced by each other. Therefore, by codoping Y^{3+} ions into the Er^{3+}-doped SiO_2 network, we believe that the –Er–O–Er–O–Er– bonding structure can be possibly changed into –Er–O–$(Y–O)_n$–Er–, which indicates that the average interionic distance between Er^{3+} ions can be enlarged. Additionally, the FTIR spectra (see Fig. 4) shows that the addition of a large number of Y^{3+} codopant could destroy the network of SiO_2, leading to an increase of non-bridging oxygen groups in the SiO_2 matrix as observed in the Er^{3+}-doped SiO_2 system by Al^{3+} codoping.[10–13] Some works reported that the non-bridging oxygen groups can reduce the tendency of the Er^{3+} ions to cluster.[10,13] According to the above-mentioned mechanism, the Y^{3+} codopant plays an important role in increasing the dispersion and solubility of Er^{3+} ions in the amorphous Er^{3+}–Y^{3+} codoped SiO_2 systems, which results in a reduction of the concentration quenching effect and an increase of PL intensity.

These explanations are very consistent with our experimental results evidenced in Fig. 9. When the Y^{3+} codoping concentration is 0 and 10 mol%, the variation of PL intensity shows the phenomenon: $I_{(1\%)} \cdot I_{(5\%)} \cdot I_{(10\%)}$ [where $I_{(1\%)}$ represents the PL intensity of the sample with 1 mol% Er^{3+} doping dose]. However, for the 20 mol% Y^{3+} codoping concentration, the phenomenon changes to $I_{(5\%)} \cdot I_{(10\%)} \cdot I_{(1\%)}$. This indicates that 10 mol% Y^{3+} codoping concentration is still not enough to disperse Er^{3+} ions very well and a large amount of Er^{3+} ions (5 and 10 mol%) still have access to form clusters. When a 20 mol% Y^{3+} codoping concentration was used, however, the influence of the concentration quenching effect on $I_{(5\%)}$ and $I_{(10\%)}$ can be considerably reduced.

For the sample with Y^{3+} concentration above 30 mol%, as the poorly crystalline pyrosilicate phase ($Er_xY_{2-x}Si_2O_7$) was crystallized in the host matrix, it can be assumed that the Er^{3+} ions are located in the $Y_2Si_2O_7$ matrix. If the Er^{3+} ions were postulated to randomly disperse in the $Er_xY_{2-x}Si_2O_7$ phases, then the average spatial distance between Er^{3+} ions should be enlarged because some Er sites were occupied by Y^{3+} ions. This indicates that the concentration quenching effect can be reduced and hence the PL intensity is enhanced for the Er^{3+} (5–10 mol%)–Y^{3+} (30–50 mol%) codoped SiO_2 samples. Therefore, the addition of a large amount of Y^{3+} (30–50 mol%) codopant still efficiently disperses the Er^{3+} (5–10 mol%) ions, which can offset the PL intensity loss resulting from the symmetry effect of the Er site.

5. Conclusion

Er^{3+}–Y^{3+} codoped SiO_2 powdered bulks were prepared by a sol–gel process. The maximum ~1.54 μm PL intensity was obtained for the Er^{3+} (10 mol%)–Y^{3+} (50 mol%) codoped SiO_2 sample annealed at 985 °C. This can be attributed to the competition between the content of hydroxy groups and Er site symmetry. Below 985 °C, the content of hydroxy groups plays an important role in PL intensity. On the other hand, above 1000 °C, the highly crystalline $Er_xY_{2-x}Si_2O_7$ phase forms and the local environment around the Er^{3+} ions becomes more symmetrical, resulting in reduced PL intensity and better resolved PL spectra. Additionally, the Y^{3+} codopant not only affects the crystallization behavior of the Er^{3+}–Y^{3+} codoped SiO_2 sample but also modifies the bonding environment of Er^{3+} ions, which leads to an enlarged interionic distance between two nearby Er^{3+} ions and a wider diversity of Er^{3+} bonding sites. Therefore, a larger bandwidth of ~1.54 μm PL spectrum with improved efficiency is obtained for the Er^{3+}–Y^{3+} codoped SiO_2 system.

Acknowledgements

The authors would like to thank the National Science Council of the Republic of China for financially supporting this research under Contract No. NSC-89-2216-E-009-034. Dr H. Y. Lee and Dr J. F. Lee of the Synchrotron Radiation Research Center are appreciated for EXAFS measurements and helpful discussions.

References

1 M. J. Weber, *J. Non-Cryst. Solids*, 1990, **123**, 208.
2 B. Pedersen, W. J. Miniscalco and R. S. Quimby, *IEEE Photonics Technol. Lett.*, 1992, **4**, 446.
3 R. Reisfeld and Y. Eckstein, *J. Chem. Phys.*, 1975, **63**, 4001.
4 W. F. Krupke and J. B. Gruber, *J. Chem. Phys.*, 1963, **39**, 1024.
5 W. F. Krupke and J. B. Gruber, *J. Chem. Phys.*, 1964, **41**, 1225.
6 E. Bescher and J. D. Mackenzie, *Mater. Sci. Eng. C*, 1998, **6**(2–3), 145.
7 K. Kojima, K. Tsuchiya and N. Wada, *J. Sol–Gel Sci. Tech.*, 2000, **19**, 511.
8 B. R. Judd, *Phys. Rev.*, 1962, **127**, 750.
9 R. M. Moon, W. C. Koehler, H. R. Child and L. J. Raubenheimer, *Phys. Rev.*, 1968, **176**, 722.
10 K. Arai, H. Namikawa, K. Kumata, T. Honda, Y. Ishii and T. Handa, *J. Appl. Phys.*, 1986, **59**, 3430.
11 C. K. Ryu, H. Choi and K. Kim, *Appl. Phys. Lett.*, 1995, **66**, 2496.
12 B. J. Ainslie, S. P. Craig and S. T. Davey, *Mater. Lett.*, 1987, **5**, 143.

13 Y. Zhou, Y. L. Lam, S. S. Wang, H. L. Liu, C. H. Kam and Y. C. Chan, *Appl. Phys. Lett.*, 1997, **71**, 587.
14 ASTM JCPDS International Centre for Diffraction Data, 1997 [Ref.: 24-0062: Pfoertsch].
15 ASTM JCPDS International Centre for Diffraction Data, 1997 [Ref.: 32-1448 and 40-0034: Pfoertsch].
16 A. M. Efimov, *J. Non-Cryst. Solids*, 1996, **203**, 1.
17 L. G. Hwa, S. L. Hwang and L. C. Liu, *J. Non-Cryst. Solids*, 1998, **238**, 193.
18 A. A. Salem, R. Kellner and M. Grasserbauer, *Glass Technol.*, 1994, **35**, 135.
19 N. A. El-Shafi and M. M. Morsi, *J. Mater. Sci.*, 1997, **32**, 5185.
20 T. Ishikawa and S. Akagi, *Phys. Chem. Glasses*, 1987, **19**, 108.
21 K. Sun, W. H. Lee and W. M. Risen, Jr, *J. Non-Cryst. Solids*, 1987, **92**, 145.
22 R. F. Bartholomew, B. L. Butler, H. L. Hoover and C. K. Wa, *J. Am. Ceram. Soc.*, 1980, **63**, 481.
23 K. Hafidi, Y. Ijdiyaou, M. Azizan, E. L. Ameziane, A. Outzourhit, T. A. Nguyen and M. Brunel, *Appl. Surf. Sci.*, 1997, **108**, 251.
24 Y. I. Smolin and Y. F. Shepelev, *Acta Crystallogr. Sect. B: Struct. Crystallogr. Cryst. Chem.*, 1970, **26**, 484.
25 L. L. Lee and D. S. Tsai, *J. Mater. Sci. Lett.*, 1994, **13**, 615.
26 W. V. Moreshead, J. R. Noguès and R. H. Krabill, *J. Non-Cryst. Solids*, 1990, **121**, 267.
27 A. Polman, *J. Appl. Phys.*, 1997, **82**, 1.
28 Y. Yan, A. J. Faber and H. de Waal, *J. Non-Cryst. Solids*, 1995, **181**, 283.
29 E. Snoeks, P. G. Kik and A. Polman, *Opt. Mater.*, 1996, **5**, 159.
30 M. Benatsou, B. Capoen, M. Bouazaoui, W. Tchana and J. P. Vilcot, *Appl. Phys. Lett.*, 1997, **71**, 428.
31 J. Phalippou, T. Woignier and J. Zarzycki, in *Ultrastructure Processing of Ceramics, Glasses and Composites*, Eds. L. L. Hench and D. R. Ulrich, Wiley, New York, 1984, p. 70.
32 D. L. Adler, D. C. Jacobson, D. J. Eaglesham, M. A. Marcus, J. L. Benton, J. M. Poate and P. H. Citrin, *Appl. Phys. Lett.*, 1992, **61**, 2181.
33 C. Piamonteze, A. C. Iñiguez, L. R. Tessler, M. C. Martins Alves and H. Tolentino, *Phys. Rev. Lett.*, 1998, **81**, 4652.
34 A. Terrasi, G. Franzò, S. Coffa, F. Priolo, F. D'Acapito and S. Mobilio, *J. Appl. Phys.*, 1997, **70**, 1712.